Analyst

RSC Publishing

PAPER

Digital compressive chemical quantitation and hyperspectral imaging

Cite this: *Analyst*, 2013, **138**, 4982

David S. Wilcox,[a] Gregery T. Buzzard,[b] Bradley J. Lucier,[bc] Owen G. Rehrauer,[a] Ping Wang[a] and Dor Ben-Amotz*[a]

Received 12th February 2013
Accepted 20th June 2013

DOI: 10.1039/c3an00309d

www.rsc.org/analyst

Digital compressive detection, implemented using optimized binary (OB) filters, is shown to greatly increase the speed at which Raman spectroscopy can be used to quantify the composition of liquid mixtures and to chemically image mixed solid powders. We further demonstrate that OB filters can be produced using multivariate curve resolution (MCR) to pre-process mixture training spectra, thus facilitating the quantitation of mixtures even when no pure chemical component samples are available for training.

1 Introduction

Modern analytical applications, including hyperspectral imaging and online monitoring, routinely generate large, high dimensional data sets. In many cases, however, the relevant chemical information resides in a much lower dimensional space. This chemical information is conventionally extracted by projecting the measured data (*e.g.*, a spectrum) onto a more informative dimension (*e.g.*, a concentration space) that can be used for classification or quantitation. Consequently, the time required to obtain full-spectral data with sufficient signal-to-noise ratio ultimately limits the speed at which the important lower dimensional information can be acquired. Compressive detection spectroscopy overcomes this limitation by adapting the measurement process to the problem, in order to directly detect the lower dimensional information of interest. In this study we extend our recently developed optimized binary (OB) compressive detection strategy[1] to demonstrate that it can be used to rapidly measure the concentration of liquid mixtures and generate chemical images of mixed powders.

Compressive detection spectrometers[1–10] incorporate multivariate optical elements, such as a liquid-crystal spatial light modulator or digital micromirror device (DMD), and use a single channel detector in place of a multi-channel detector such as a charge-coupled-device (CCD) camera.[11,12] In other words, compressive detection is achieved by transmitting (or reflecting) the light of interest through a programmable optical filter whose shape is optimized so as to obtain the concentrations of the chemical components of interest with a maximum signal-to-noise ratio in a given total detection time, particularly when that time is sufficiently short that conventional CCD-based full spectra detection is not feasible.

The OB compressive detection method relies on binary optical filters (produced using a holographic optical volume grating and a DMD) obtained by minimizing the mean square error in estimates of the photon emission rates, and thus the corresponding concentrations (or total amounts) of the chemical components of interest.[1] We previously demonstrated that OB compressive detection can be used to accurately distinguish (classify) pairs of liquids in time scales of microseconds to milliseconds (and that it outperforms alternative spectral classification strategies based on total least squares). A key mathematical result of that study was that the optimal filters for minimizing concentration error were "nearly" binary, such that rounding all non-binary entries of each filter satisfactorily provided (near-)optimal binary filters. Such filters are naturally suited for use with a DMD, in which the mirrors direct light either towards or away from a single-channel, photon-counting, amplified photodiode detector.

Here we extend our previous work to study quantitation and hyperspectral imaging using OB compressive detection. Accurate quantitation of binary and ternary liquid solutions is demonstrated on 10–100 ms time scales. Moreover, a raster scanning technique is implemented to rapidly scan the microscope field of view to image mixtures of sugars on 0.1–10 ms per pixel time scales. Finally, we show that multivariate curve resolution can be used to generate filters when no pure chemical component samples are available.

2 Methods

2.1 Binary filter model

The following is a brief overview of key results of the mathematical model used to produce optimal binary filters (which have previously been described in greater detail).[1] We assume

[a]*Purdue University, Department of Chemistry, West Lafayette, IN, USA. E-mail: bendor@purdue.edu; Tel: +1 765 494 5256*

[b]*Purdue University, Department of Mathematics, West Lafayette, IN, USA*

[c]*Purdue University, Department of Computer Science, West Lafayette, IN, USA*

that all photons are emitted from n known spectra and are counted by the detector as Poisson random variables. We also assume that each photon can be classified into one of N energy bins. If these known spectra are normalized to unit area and compiled into the columns of a matrix P, then the rates that photons "hit" all energy bins can be expressed as $P\bar{\Lambda}$, where the components of the vector $\bar{\Lambda}$ are the mean photon rates emitted by each chemical species.

The speed of compressive detection is realized by finding a set of optical transmission filters $F\,(0 \leq F_{ij} \leq 1)$, which, for each measurement j (associated with the j^{th} column of F), project certain wavelengths onto a single channel detector. We assume for simplicity that the number of measurements M equals the number of possible chemical species n. The photons reaching the detector are modeled as Poisson random variables with means and variances equal to $TF^{\text{T}}P\bar{\Lambda}$, where T is a diagonal matrix indicating the normalized integration time of each measurement filter ($\sum T_{ii} = 1$). The measured photons emerging through the filters are denoted $\hat{\mathbf{x}}$. Defining $A = F^TP$ and $B = A^{-1} = (F^TP)^{-1}$, the rates are recovered by

$$\bar{\Lambda} = BT^{-1}\hat{\mathbf{x}} \tag{1}$$

We seek filters such that $\hat{\Lambda}$ is close to $\bar{\Lambda}$. Thus, we formulate our optimization problem to minimize the following expression:

$$E(\|BT^{-1}\hat{\mathbf{x}} - \bar{\Lambda}\|^2) \tag{2}$$

It can be shown[1] that in the absence of read noise, this expression can be written explicitly as

$$\left(\sum_{i=1}^{M} ||B\mathbf{e}_i|| \sqrt{(A\bar{\Lambda})_i}\right)^2, \tag{3}$$

where $B\mathbf{e}_i$ is the i^{th} column of B. Minimizing this expression subject to $A = F^TP$, $B = A^{-1}$, and $0 \leq F_{ij} \leq 1$ for all i, j yields optimal filters with at most $n - 1$ non-binary channels. These channels are subsequently rounded to produce the OB filters. The matrix of relative measurement times T can be calculated from A, B, and $\bar{\Lambda}$.[1]

2.2 Compressive detection spectrometer

The compressive detection spectrometer used in this study is comprised of two main parts: The first part, shown in Fig. 1, contains the optical excitation and Raman scattered light collection components. The second part houses the DMD, volume holographic grating, photon counting module, and associated optics (not shown in Fig. 1). The latter optical set-up has previously been described in detail.[1]

In the present studies we have modified the Raman back-scattering optics to include x–y scanning mirrors (Galvonometer, GVS002, Thorlabs) and transfer lenses (AC254-150-B-25.4 mm, $f = 150.0$ mm, Near IR Achromat, Thorlabs) to rapidly raster-scan the excitation/collection point within the sample (see Fig. 1). The distance between the raster scanning optics (galvonometer mirrors) and the first transfer lens, and

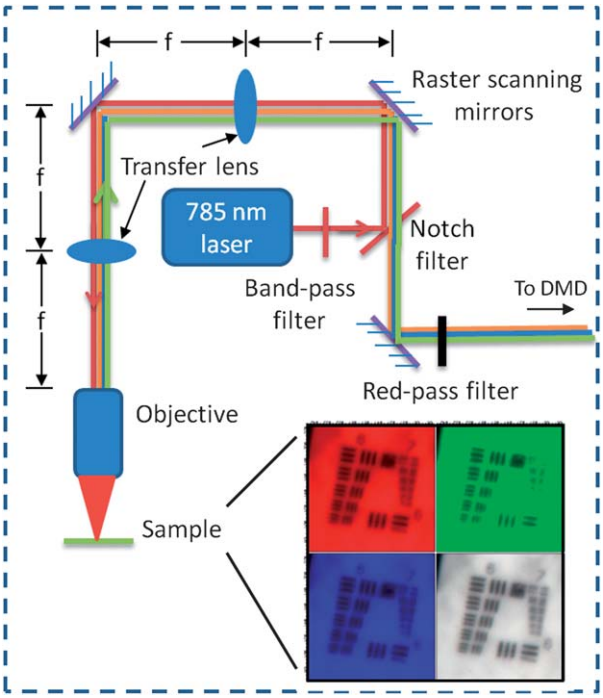

Fig. 1 Schematic of the Raman excitation optics, including the raster scanning mirrors and transfer lenses used to produced chemical images. The red, green, and blue (RGB) inset panels show independently measured images of a USAF bar target (the periodicity of the target lines in group 6 ranges from 4.39 μm to 7.81 μm). The image in the lower right-hand panel is a composite obtained by superposing the three RGB images (see text for details).

that between the second transfer lens and the microscope objective, are each equal to the transfer lens focal length f, while the distance between the two transfer lenses is $2f$ (the location of the mirror in the upper-left of Fig. 1 is not critical). This configuration ensures that the laser spot always remains centered at the back of the objective as the x–y raster scanning mirrors move, and that the back scattered light sent to the DMD-associated optics remains stationary (independent of the raster mirror position).

When using a 20× microscope objective (NA = 0.4), the mirrors can scan a 100 × 100 pixel region (of ~0.25 mm^2 area) at speeds of up to ~5 frames per second (which is higher than is possible with a mechanical stage). The spatial resolution of ~5 μm was determined with a USAF bar target, shown in Fig. 1. Bar target images were acquired by setting all the DMD mirrors to the on position and integrating each point for 1 ms. The three RGB colored bar-target images shown in Fig. 1 were produced from three independently collected data sets that were subsequently combined to produce the lower right bar-target image. These independently collected images are registered to within an average displacement of about 0.01 pixels, as determined by comparing the registry of 30 bar target images (as described in Section 2.6).

Full spectral measurements, used as input training spectra to produce OB filters, were acquired by notch scanning sequential vertical stripes of 8 or 16 DMD mirrors (corresponding to a spectral vibrational frequency resolution of ~15

and ~30 cm^{-1}, respectively) and integrating for 1 s per block. OB compressive detection measurements were obtained by setting vertical stripes (8 or 16 DMD mirrors wide) to either the on or off position, as specified by the OB filters (produced either using background subtracted pure component spectra or component spectra obtained as described in Section 2.4).

2.3 Removing background

A background emission originating from the objective lens and intervening optics is present in all measured spectra. If the background is constant in shape and intensity (as is typically the case when performing point measurements on clear liquid samples), then we have previously demonstrated[1] that compressive detection can be used to eliminate the background photon contributions from those chemically relevant photons. Thus, for the analysis of liquid mixtures (as described in Sections 3.1 and 3.2) the training set is comprised of the spectra of each pure chemical compound (each of which include the background spectrum), as well as the isolated background spectrum (obtained by removing the sample from the collection volume of the microscope objective).

For the analysis of solid powders and mixtures (as described in Section 3.3), assumptions regarding constant background spectrum intensity are no longer applicable (in part due to local variations in the backscattering from powdered samples). Such background intensity variations were handled by treating the background signal as an independent spectral component. Thus, the training set for solid powered samples could be comprised of the pure (sample free) background spectrum and pure chemical component spectra obtained after subtracting the background by minimizing the isolated background peak at ~1875 cm^{-1}. An alternative way to obtain background free training spectra is to use multivariate curve resolution (MCR) to decompose a series of pure powder spectra into pure background and pure chemical spectra (as described in Section 2.4). The former manual subtraction method produces chemical spectra which are virtually identical to those obtained with multivariate curve resolution; see Fig. 5.

2.4 Multivariate curve resolution

The speed of the compressive detection spectrometer is fully realized when the spectra of all pure components are known. However, if only composite samples are available (see Section 3.4), then training spectra can be acquired with multivariate curve resolution (MCR). The goal of MCR is to decompose a set of mixture data into a product of pure concentrations and spectra with little or no *a priori* information. The MCR-derived spectra can subsequently be used as training spectra for finding OB filters.

We have employed entropy minimization (EM), as described in Section 3.4, to find pure spectral estimates from mixture spectra taken at arbitrary pixels. EM is an MCR technique based on singular value decomposition of a matrix of mixture data.[13] For samples containing n distinct chemical component, the first n eigenvectors should contain all of the chemical information (and the subsequent eigenvectors contain only noise). The first n eigenvectors are linear combinations of the pure components; these must be rotated to obtain pure spectral estimates. Since many different rotations are possible, EM requires that, in addition to non-negativity, the rotated eigenvectors must have a minimum Shannon spectral entropy. In essence, this minimization criteria produces component spectra that have the simplest, narrowest, and most separated features. We use simulated annealing to find the rotation matrix elements that minimize the normalized second or fourth derivative of the pure spectral estimates for moderately or highly overlapping spectra, respectively. The derivative spectra were pre-treated with Savitsky–Golay smoothing (with a 7 point window width). Since the spectral profile of the background is known, it was fixed in the minimization algorithm by first finding the linear combination of eigenvectors that reproduced the known background spectra and then subsequently fixing the corresponding row in the rotation matrix. Fixing one component leads to better estimates of the remaining pure component spectra.

2.5 Materials

Samples of 1-hexene (97%), *m*-xylene (99+%), *o*-xylene (99+%), *p*-xylene (99+%), and D-(−)-fructose (99%) were purchased from Sigma-Aldrich. D-(+)-sucrose and hexanes (min 95% sum of 5 isomers, total hexanes, and methylcyclopentane determined by GC-MS) were purchased from Mallinckrodt Chemicals and D-(+)-glucose (99.5%) was purchased from Fluka. All samples were used without further purification. Liquid samples were prepared in spectroscopic cuvettes. Solid samples were ground using a mortar and pestle and then distributed either side by side (Sections 3.3 and 3.4) or mixed (Section 3.4) on a gold microscope slide substrate.

2.6 Computations and software

All experiments were implemented in Labview 9.0 (National Instruments). The drivers for the raster-scanning mirrors (Servo Drive Board) were controlled by a DAQ interface (National Instruments, USB-6212BNC). The DAQ interface also features an on-board counter that is used for counting the TTL pulses output by the photon counting photodiode module (PerkinElmer, SPCMCD2969PE). The DMD (DLP D4000, Texas Instruments) connects *via* USB interface, and is controlled through software available from Texas Instruments (Load Blocks.vi, DDC4100). Matlab R2012a (MathWorks, Inc.) was used to generate filters in a program built around the fmincon.m function from the Optimization Toolbox. The Matlab program used in this work is available upon request (see http://www.math.purdue.edu/~buzzard/software/). The evaluation of the image registration was also performed in Matlab R2012a using the imregister.m function from the Image Processing Toolbox. Images were registered to a reference bar target image using only translational movements in a monomodal configuration for intensity-based registration. Entropy minimization was also performed in Matlab R2012a.

Data was further processed in IgorPro 6.04 (WaveMetrics). In Sections 3.3 and 3.4, the chemical images were constructed by first setting all pixels with negative estimated absolute photon

rates, or spectral weights, to zero (note that the expression in eqn (2) allows negative estimated rates, as $\hat{\Lambda}$ is an unbiased estimate of $\bar{\Lambda}$; the occurrence of such negative estimates varies inversely with integration time and with component concentration). In the 1 ms per pixel chemical images of Fig. 6 (middle panel) and 7, the absolute $\hat{\Lambda}$ at the i^{th} pixel of the n^{th} component were mapped to an 8 bit grayscale as follows:

$$\text{pixel}_{i,n}^{1\text{ ms}} = \hat{\Lambda}_{i,n}^{1\text{ ms}} / \max_j(\hat{\Lambda}_{j,n}^{1\text{ ms}}) \times 255$$

where the maximum rates were 2.8083×10^6 and 1.6106×10^6 photon s^{-1} for fructose and glucose, respectively, in Fig. 6 (middle panel). The maximum rates in Fig. 7 were of similar magnitude. In the 0.1 ms per pixel image of Fig. 6 (far right panel), $\hat{\Lambda}_{i,n}$ was mapped to an 8 bit grayscale according to

$$\text{pixel}_{i,n}^{0.1\text{ ms}} = \min\left[255,\ \text{round}\left[\hat{\Lambda}_{i,n}^{0.1\text{ ms}} / \max_j(\hat{\Lambda}_{j,n}^{1\text{ ms}}) \times 255\right]\right],$$

where $\max_j(\hat{\Lambda}_{j,n}^{1\text{ ms}})$ is the maximum photon rate of the corresponding component in the 1 ms per pixel image (this adjusted the brightness of the 0.1 ms per pixel image). The final cyan and yellow image is given by the RGB vector (r,g,b)

$$\text{RGBpixel}_i = (\text{pixel}_{i,1},\ \max(\text{pixel}_{i,1},\ \text{pixel}_{i,2}),\ \text{pixel}_{i,2}).$$

A similar normalization was applied in Fig. 9, but with all panels normalized by $\max_j(\hat{\Lambda}_{j,n}^{10\text{ ms}})$.

3 Results and discussion

The relative contributions of multiple components to the Raman light emanating from a liquid sample can be used to obtain the mole fraction of each component. If $\hat{\Lambda}_i$ is the experimental estimate of the detected photon rate arising from component i, then the relative intensity contribution of that component to the light collected from the mixture is $\hat{\Lambda}_i / \sum_i \hat{\Lambda}_i$.

In order to obtain the apparent mole fraction of each component in a mixture, the measured rates must each be multiplied by an appropriate weighting factor to obtain

$$\chi_i = \frac{w_i \hat{\Lambda}_i}{\sum_i w_i \hat{\Lambda}_i}.$$

If the weighting factors are defined as $w_i = M_i / \Lambda_i^{\max}$ (where M_i is the molarity of the i^{th} pure liquid, and $\Lambda_i^{\max}$ is the average rate obtained from a sample consisting purely of component i), then χ_i becomes an experimental estimate of the mole fraction of each component. Note that variations in the excitation laser intensity (as well as optical alignment, *etc.*) may change the values of $\Lambda_i^{\max}$ and $\hat{\Lambda}_i$. However, as long as the latter rates are measured under identical conditions (*e.g.*, with the same laser intensity, optical alignment, *etc.*) then such variation will not affect the values of χ_i.

3.1 Two-component liquids

The spectra of hexanes and 1-hexene are shown in panels (a) and (b) in Fig. 2. These liquid samples were selected because they are moderately difficult to distinguish due to the degree of spectral similarity, and because such mixtures are of practical relevance to the determination of the degree of unsaturation of cooking oils. Each of the measured spectra included background features arising from the objective lens (shown in panel (c)). The grey bars in panels (a)–(c) of Fig. 2 indicate the locations of mirrors that are turned on in the OB filter associated with each spectrum. Determining the photon rates of each sample requires applying all three filters and measuring the resulting total number of photons reflected towards the detector by each filter. Since the spectra overlap at many wavelengths, each filter collects photons from all components in the system, and a linear combination of these measured photons produces corresponding photon rates for each component (see eqn (1)). The relative (fractional) integration times for each filter, determined by minimizing eqn (3), were 0.41, 0.48, and 0.10 for the filters associated with hexanes, 1-hexene, and the background, respectively.

For this system, the photon rates of the pure components were measured in 100 ms (total integration time, which does not include the DMD mirror switching time of ~30 ms) and converted into mole fraction concentrations. Panel (d) of Fig. 2 compares 11 prepared mixtures of hexanes and 1-hexene, with mole fractions ranging from zero to one. The diamonds represent the mean of 1000 independent measurements. The latter mean mole fractions are all within 1% of the dashed ideal line. The error bars represent two standard deviations above and below the mean, or ~0.04 mole fraction per mixture. The precision of the quantitation depends on the integration time. The inset of panel (d) shows that the log of the standard deviation as a function of the log of the integration time has a slope of ~−0.5, indicating that the noise scales as the square root of the signal, as expected from Poisson photon counting statistics.

3.2 Three-component liquids

Here we describe the quantitation of three-component liquid samples consisting of mixtures of xylene isomers. These ternary liquid mixtures were selected in part because they have been previously used in demonstrating the performance of a DMD-based compressive detection prototype.[4] In the latter work, various feature selection methods were tested with the goal of finding the wavelengths suitable for quantifying mixtures with less than 5% error. A method that measures several peak intensities simultaneously, called the "sum of characteristic peaks of a component" method, was found to produce the lowest error (less than 3%) in the shortest time (approximately 3 s of chemical quantitation and 3 s for background correction). Here we demonstrate that our OB compressive detection strategy (*i.e.* both the instrument and mathematical filter design) can achieve a similar accuracy over 100 times faster.

Panels (a)–(d) in Fig. 3 show the spectra of *m*-, *o*-, *p*-xylene, and the background, respectively, along with associated OB filters (indicated by the vertical grey regions). The linear plot in Fig. 4 compares the measured (vertical axis) and actual

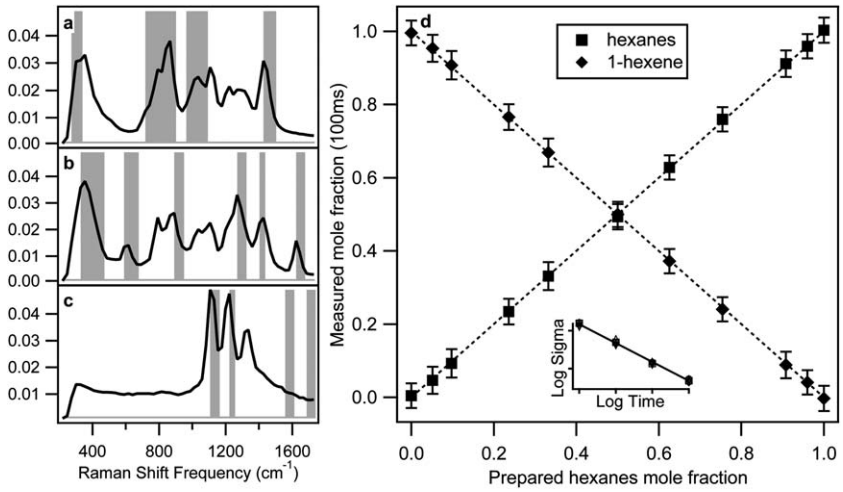

Fig. 2 Comparison of the spectra of hexanes + background, 1-hexene + background, and the background are shown with the associated filters (gray bars) in panels (a)–(c). The constant background contribution is removed from these liquid component spectra as previously described.[1] Panel (d) shows the quantitation results obtained from eleven solutions of hexanes and 1-hexene, with mole fraction ranging from 0 to 1, and measured for 100 ms per solution. The error bars represent two standard deviations of 1000 measurements, which is ~4 mole%. The inset of panel (d) shows the decrease in standard deviation with integration time ranging from 1 ms to 1 s (and the resulting best fit line has a slope of −0.497 and a correlation coefficient of −0.997).

(horizontal axis) mole fraction for a series of 3 ternary mixtures. Xylene mixtures were measured using the four OB filters in Fig. 3 with relative (fractional) times of 0.39, 0.33, 0.22, 0.06 for the filters in panel (a), (b), (c), and (d), respectively, with a total integration time of 10 ms (for all four filters). The average concentrations obtained from 1000 independent measurements were again found to be within 1% of the prepared mole fractions. The errors bars in Fig. 4 represent two standard deviations above and below the mean (or ~4 mole%). Although the measure of error reported by Quyen *et al.*[4] was slightly different (the authors built a regression model and reported the root mean squared error of prediction of a test data set), the present results demonstrate that accurate quantitation of this xylene system is possible in 10 ms, which is over 100 times faster than in the previously reported DMD-based compressive detection strategy.

It is interesting to note that the spectra of *m*- and *o*-xylene (Fig. 3, panels a and b) have several overlapping bands, whereas the bands of *p*-xylene (Fig. 3, panel c) are largely isolated. Consequently, the standard deviation (error bars in Fig. 4) of the *p*-xylene's concentration in each mixture is smaller than those of the other isomers. This is also reflected in the data cube inset, which shows that the variance is larger in the two dimensions corresponding to *m*- and *o*-xylene than in the *p*-xylene direction.

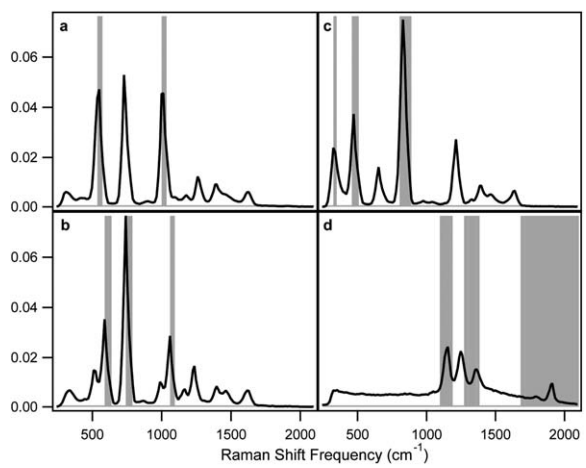

Fig. 3 Comparison of the spectra of *m*-xylene + background (a), *o*-xylene + background (b), *p*-xylene + background (c), and the background (d) with associated filters (gray bars).

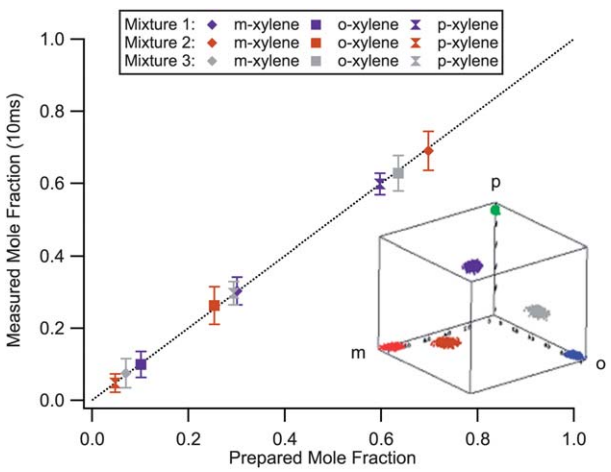

Fig. 4 Quantitation results obtained from liquid mixtures of three xylene isomers. The mole fractions obtained in 10 ms per solution are plotted as a function of the actual mole fractions. The errors bars represent two standard deviations, or ~4 mole%. The inset shows the same mixture mole fraction results plotten in a cube, with each axis corresponding to a different xylene component. The measured pure component mole fractions are shown as red, green, and blue distributions, and the location of each mixture depends on the relative amount of each component.

3.3 Hyperspectral imaging

Here we demonstrate the application of our OB compressive detection strategy to the imaging of mixtures of two sugars, fructose and glucose, using as little as ~30 photons per pixel. These samples were selected because they have an identical (white powder) appearance and moderately overlapped Raman spectra, and thus represent a chemical imaging application of intermediate challenge. In Section 3.4, we apply compressive detection to distinguish the highly overlapping spectra of glucose and sucrose. Unlike liquid samples, various factors including grain size and relative crystal orientation affect the amount of scattered light, and thus it is more difficult to determine the number of photons emitted per unit sample. The chemical images described in this section were constructed by mapping the normalized and scaled measured photon rates of each component at each pixel (see Section 2.6 for more details).

The spectra of fructose, glucose, and the background emission are shown in Fig. 5. The correlation coefficient (normalized dot product) of these two sugar spectra is 0.85. Fig. 6 shows images of fructose and glucose placed side by side in the imaging field of view. The two sugars cannot be distinguished from each other in the "white light" image (taken by setting all the DMD mirrors to the "on" position). The spatial distribution of each sugar becomes clear in the chemical images shown in the two colored images in Fig. 6 (with fructose in yellow and glucose in cyan). These 300 × 300 pixel chemical images were obtained using OB filters shown in panels (a)–(c) of Fig. 5, with relative (fractional) times of 0.37, 0.35, and 0.28, respectively. The chemical images in the middle and far right of Fig. 6 were measured with total times 1 ms per pixel and 0.1 ms per pixel, respectively, (for a total integration time of ~90 s and ~9 s per image, respectively). Note that the filter switching time of 30 ms is in this case negligible, since the images are collected by scanning the entire 300 × 300 image with each OB filter. The average number of measured photons per filter in the far right image of Fig. 6 was only ~10.

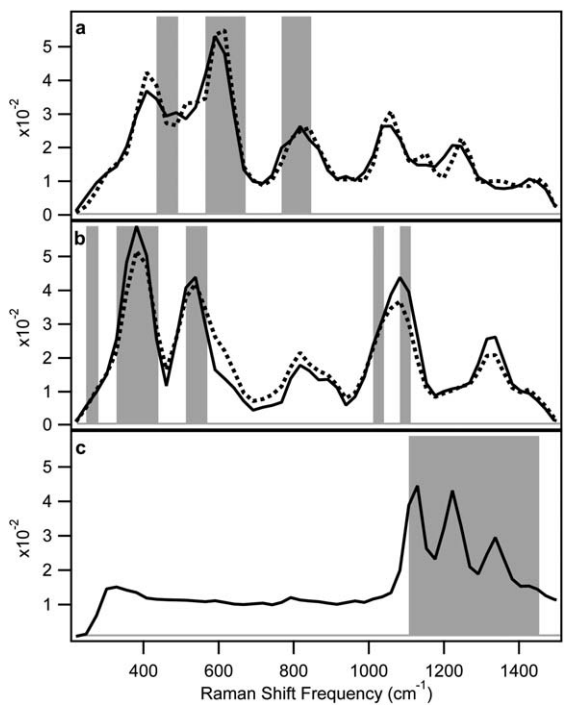

Fig. 5 Comparison of the Raman spectra and OB filters of pure fructose (a), pure glucose (b), and the background. The solid and dashed curves compare the corresponding directly measured (background-subtracted) spectra and MCR-derived spectra, respectively (see Sections 2.3, 2.4, and 3.4). The gray bars indicate the OB filters obtained from the directly measured pure component spectra (solid curves).

3.4 Multivariate curve resolution in imaging

In many imaging applications of biological, geological, or archaeological relevance, pure samples are not readily available (or perhaps even known). However, it is always possible to obtain mixture spectra from such samples by collecting full spectra from different locations within a sample. Here we demonstrate that multivariate curve resolution (MCR) techniques[14] can be used to estimate pure training spectra from mixture data, with little or no *a priori* information regarding the spectral shapes or number of compounds. More specifically, given a representative collection of mixture spectra from various locations in a sample, MCR can be used to extract component spectra from which OB filters can be generated, and then used to rapidly collect a chemical image of the entire sample (or a series of samples). Note that this approach has some similarities to that used by Perera *et al.* to obtain a hyperspectral chemical image of plant tissue.[15] However, the latter study obtained chemical images by post-processing of full CCD spectral measurements, rather than using a high speed compressive detection strategy.

The performance of this MCR approach was first evaluated using a mixture of fructose and glucose powders. Full spectra were taken from four arbitrarily selected locations within the mixed pure powder. These spectra and the background were decomposed into pure spectral estimates using the entropy minimization MCR algorithm (as described in Section 2.4). The resulting MCR spectral estimates of the pure fructose and glucose spectra (dashed curves in Fig. 5) were found to be in excellent agreement with the corresponding pure spectra (solid curves in Fig. 5). The visually evident similarity of the component spectra obtained using both methods is quantitatively confirmed by the correlation coefficient of 0.99 for the two fructose spectra and 0.97 for two glucose spectra.

Fig. 7 shows a comparison of two sets of sugar powder images obtained using OB filters generated using either spectra of the two pure sugars (left) or using the corresponding MCR-derived component spectra (right). Clearly, both methods produce similar images. The correlation coefficient of the two upper images is 0.93 for fructose and 0.90 for glucose while that for the two lower images is 0.95 for fructose and 0.92 for glucose, indicating there is little systematic or random (noise) differences between the sets of images.

The compressive detection and MCR strategies can also be applied to more difficult chemical imaging problems. Fig. 8

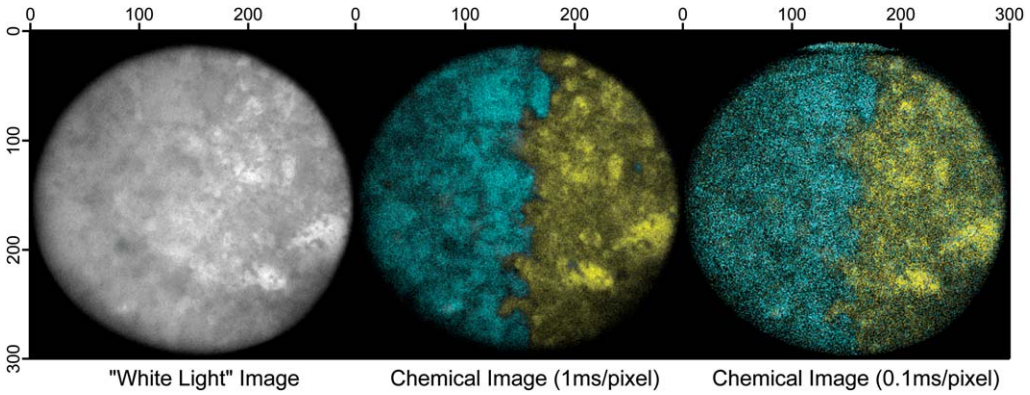

Fig. 6 The "white light" image of a side-by-side mixture of fructose and glucose (far left) was measured by turning all of the DMD mirrors to the "on" position at each pixel. When using OB filters, the chemical information is clearly segregated in the middle image, measured with 1 ms per pixel (with fructose in yellow and glucose in cyan). The same chemical information is still discernible in the image on the far right, which was measured with 100 μs per pixel. This latter integration time corresponds to an average of ~10 measured photons per filter, or ~30 photons per image pixel.

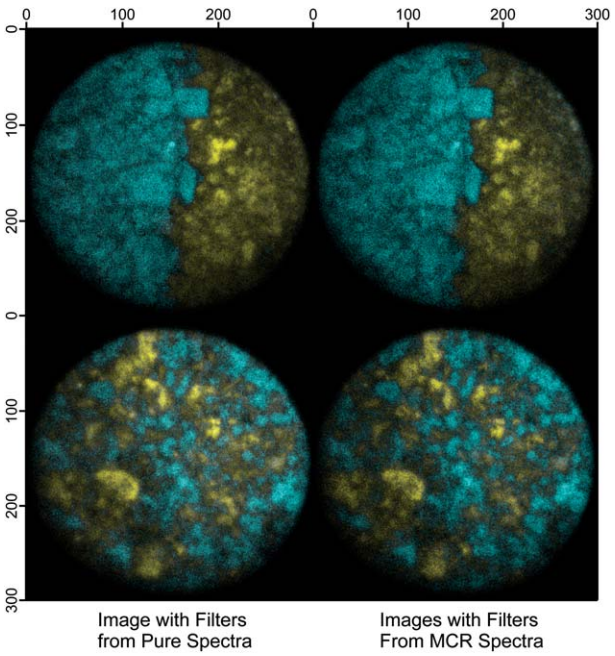

Fig. 7 Image comparison of fructose (yellow) and glucose (cyan) obtained using two different methods for finding OB compressive detection filters. The two left-hand images were obtained using filters derived from directly measured (and background-subtracted) pure component spectra. The two right-hand images were obtained using MCR-derived component spectra. The latter method does not require that pure samples are available, as pure component spectra are extracted from spectra obtained from a small number of randomly selected points within the sample of interest. All of the above images were acquired with an integration time of 1 ms per pixel.

shows a case where the Raman spectra of two chemical components, glucose and sucrose, have many component bands that are nearly coincident but differ in relative intensities (the correlation coefficient of these two spectra is 0.96). The OB filters generated from the training spectra are shown in Fig. 8, where the fractional times were 0.29, 0.44, and 0.27 for panels (a)–(c). Due to the high degree of spectral similarity, it was necessary to precisely align the optical components in order to successfully implement the OB filters on this system (we performed classification experiments on the pure glucose or pure sucrose powders to ensure the spectrometer was optimally aligned). This is in contrast to the previously demonstrated cases with a lower degree of spectral overlap (Fig. 2, 3 and 5), for which the compressive quantitation results were relatively insensitive to small misalignments of the system.

A chemical image of a mixture of glucose and sucrose obtained using OB filters is shown in Fig. 9. Here, the upper left panel was acquired at 10 ms per pixel, while the lower left panel was obtained with 1 ms per pixel. A longer total integration time is required to obtain images of comparable quality for the glucose and sucrose (top left panel of Fig. 9) than is required for fructose and glucose (top and bottom left panels of Fig. 7) due to the increased spectral overlap.

The dashed traces in Fig. 8 show the MCR decomposition spectra of glucose and sucrose obtained from eight mixture spectra taken at arbitrary locations in a mixture of glucose and sucrose powders. Note that the number of mixture spectra was increased to ensure that the highly overlapping spectra were accurately resolved. The entropy minimization results produced spectra resembling the known sugar spectra, with a correlation coefficient of 0.98 for the two glucose spectra and 0.99 for the two sucrose spectra. These MCR spectra were used to generate OB filters, and the resulting chemical images shown in the two right-hand panels Fig. 9 are again comparable with the OB filters derived from the training on the pure powders (shown in the two left-hand panels of Fig. 9). The correlation coefficient of the glucose and sucrose images at 10 ms per pixel is 0.95 and 0.98, respectively, indicating there is little systematic difference between the images. At the shorter integration time of 1 ms per pixel, the influence of increasing noise decreases the correlation coefficient of the glucose images to 0.74 and sucrose to 0.94. These sugar results demonstrate that compressive detection combined with MCR works equally well in imaging both moderately and heavily overlapped components in a mixture.

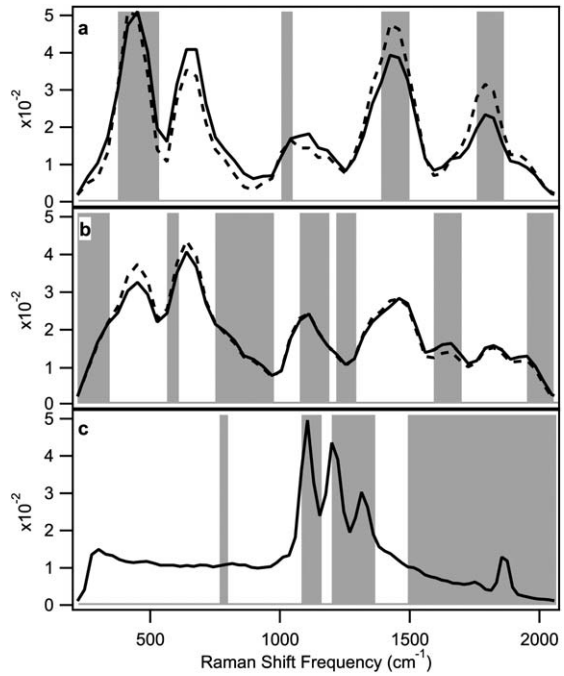

Fig. 8 Comparison of the Raman spectra and OB filters of pure glucose (a), pure sucrose (b), and the background. The solid and dashed curves compare the corresponding directly measured (background-subtracted) spectra and MCR-derived spectra, respectively. The gray bars indicate the OB filters obtained from the directly measured pure component spectra (solid curves).

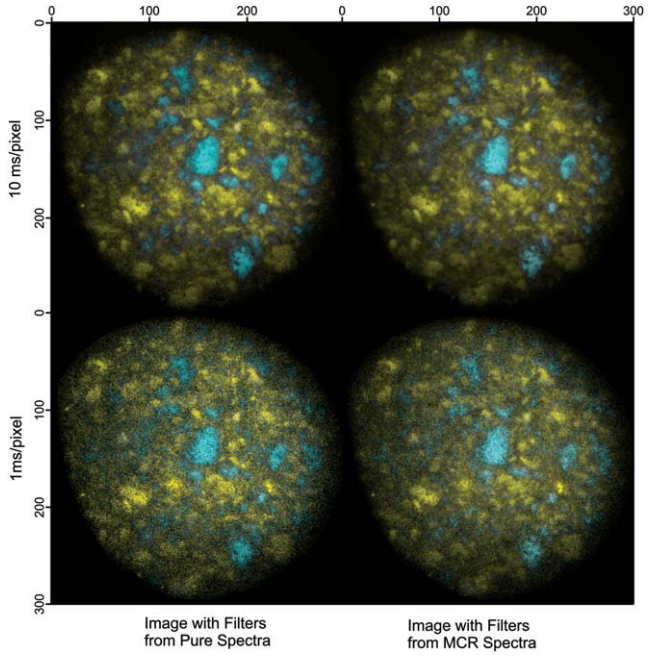

Fig. 9 Image comparison of glucose (cyan) and sucrose (yellow) obtained using two different methods for finding OB compressive detection filters and pixel integration time. The images in the left panels were obtained using filters derived from background-subtracted spectra measured from pure powders. The two right-hand images were obtained using MCR-derived component spectra. The top panels were measured with an integration time of 10 ms per pixel, while the bottom were measured with 1 ms per pixel.

4 Conclusion

We have demonstrated that the OB compressive detection strategy can be used to rapidly quantify binary and tertiary liquid mixtures, as well as to obtain chemical images of mixed powders. The results of this work demonstrate that in general there is a trade off between the degree of spectral similarity and the time required to obtain accurate results. In other words, we have found that it is possible to quantify or image mixtures containing components that are highly spectrally overlapped, but doing so requires longer integration times than mixtures with less overlapped spectra. We have further demonstrated that the OB compressive detection strategy can be combined with multivariate curve resolution to facilitate high speed chemical imaging of samples for which pure components spectra are not available. Thus, our results imply that OB compressive detection is likely to be broadly applicable to chemical quantitation and imaging, either using pure components for training or using component spectra obtained from the liquid or solid mixtures of interest for training.

Acknowledgements

This work was supported in part by the National Science Foundation (Award # IDBR 0754740 to DSW, OGR, PW, and DBA), the Office of Naval Research (Contract N00014-13-1-0394 to DBA, GTB, and BJL), and the Simons Foundation (Awards #209418 and #229816 to BJL). GTB is grateful for the hospitality of IHES during the preparation of this manuscript.

References

1 D. S. Wilcox, G. T. Buzzard, B. J. Lucier, P. Wang and D. Ben-Amotz, *Anal. Chim. Acta*, 2012, **755**, 17–27.
2 Z. J. Smith, S. Strombom and S. Wachsmann-Hogiu, *Opt. Express*, 2011, **19**, 16950–16962.
3 B. M. Davis, A. J. Hemphill, D. C. Maltas, M. A. Zipper, P. Wang and D. Ben-Amotz, *Anal. Chem.*, 2011, **83**, 5086–5092.
4 N. T. Quyen, E. Da Silva, N. Q. Dao and M. D. Jouan, *Appl. Spectrosc.*, 2008, **62**, 273–278.
5 M. N. Simcock and M. L. Myrick, *Appl. Opt.*, 2007, **46**, 1066–1080.
6 N. Uzunbajakava, P. de Peinder, G. W. t. Hooft and A. T. M. van Gogh, *Anal. Chem.*, 2006, **78**, 7302–7308.
7 M. C. Van Beek, F. J. P. Schuurmans and L. P. Bakker, *Patent: Optical analysis system using multivariate optical elements*, 2005, US 20070177240 A1.
8 M. P. Nelson, J. F. Aust, J. A. Dobrowolski, P. G. Verly and M. L. Myrick, *Anal. Chem.*, 1998, **70**, 73–82.
9 R. A. DeVerse, R. M. Hammaker, W. G. Fateley, J. A. Graham and J. D. Tate, *Am. Lab.*, 1998, **30**, 112S.
10 E. P. Wagner, B. W. Smith, S. Madden, J. D. Winefordner and M. Mignardi, *Appl. Spectrosc.*, 1995, **49**, 1715–1719.

11 J. Jacak, C. Hesch, J. Hesse and G. J. Schütz, *Anal. Chem.*, 2010, **82**, 4288–4292.
12 K. Golcuk, G. S. Mandair, A. F. Callender, N. Sahar, D. H. Kohn and M. D. Morris, *Biochim. Biophys. Acta, Biomembr.*, 2006, **1758**, 868–873.
13 Y. Zeng and M. Garland, *Anal. Chim. Acta*, 1998, **359**, 303–310.
14 A. de Juan and R. Tauler, *Crit. Rev. Anal. Chem.*, 2006, **36**, 163–176.
15 P. N. Perera, M. Schmidt, P. J. Schuck and P. D. Adams, *Anal. Chim. Acta*, 2011, **702**, 172–177.